Journal of Materials Science: Materials in Electronics (2019) 30:4279–4288
https://doi.org/10.1007/s10854-019-00720-7

Synthesis of silver bromide/graphene oxide composite and its enhanced visible light photocatalytic e□ciency and mechanism for elimination of parachlorobenzoic acid

Li-chao Nengzi[1,2] · You-zhong Zhang[2] · Jin-Hua Ma[2] · Hai-Tao Li[2] · Qingfeng Cheng[1,2,3] · Xiuwen Cheng[2,3,4]

Received: 8 October 2018 / Accepted: 8 January 2019 / Published online: 23 January 2019

In this study, silver bromide/graphene oxide (AgBr/GO) composite was synthesized by a simple ultrasonic-precipitation process. Afterwards, series of measurments demonstrated that AgBr/GO displayed improved visible light absorbance and higher photogenerated charge carriers. In addition, we proposed the enhanced visible light driven photocatalytic mechanism of AgBr/GO. Besides, AgBr/GO composite exhibits a higher PC activity (99.9%) for degradation of parachlorobenzoic acid than that of pristine AgBr within 40 min illumination. Finally, the degradation pathways of parachlorobenzoic acid were concluded. This study provides a new insight to promote the development of new fashioned photocatalytic decomposition of emerging contaminants from natural water bodies.

In recent years, with the rapid development of science and technology, the issue of environmental pollution has drawn more and more attention. Especially, the water pollution is one of the most important problems that people must face [1, 2]. To solve the increasingly serious crisis on water pollution, photocatalysis, as a prospective candidate for the use of solar energy, was regarded as a kind of effective technique for degrading organic pollutants to non-toxic small molecules and achieve no harm [3–5]. Parachlorobenzoic-acid (PCBA), as a typical organic pollutant with high toxicity, potential oncogenicity, high stability and non-degradability, was mainly coming from pesticides, herbicides, fungicides and intermediates for dyes and organic synthesis [6–8]. Once the PCBA was discharging into the environment, it will bring great harm to the ecological environment and human health [9, 10]. So far, many metallic oxides have been extensively used as promising materials for photocatalysis due to their advance and comparative large quantity [11–14]. In particular, TiO_2 has been employed widely for degradation of organic contaminants in recent years [15–17]. Nonetheless, TiO_2 nanomaterials possess wide band gap (~3.2 eV) and rapid recombination rate of photo-induced electrons (e^-) and holes (h^+) pairs, which significantly affects its photocatalytic and photoelectrochemical properties [18–20]. Thus, it is imminent and essential to develop novel photocatalysts which response for visible light.

In order to harvest solar energy effectively and economically, a great deal of interest has focused on the research of silver halides (AgX) nanomaterial in the recent year, particularly the AgBr photocatalysts with a narrow band-gap of 2.64 eV (470 nm), which show excellent photocatalytic performance in the range of visible-light [21–23]. Moreover, according to previous reports, AgBr photocatalysts show high absorptivity in a wide UV–Vis spectral range due to the strong light response [24]. That is to say, the photon would be absorbed by AgBr to generate an electron and a positive hole, which can be further used in the photocatalytic process to degrade pollution under visible light irradiation [25].

However, it was realized that the AgBr could not be used the whole photoactivity because of its large particles [26]. The composite materials could improve the AgBr dispersion in medium which favourable for the development of electron transport and photocatalytic effect. Notably, as a new carbonaceous material, Graphene (G) with two dimensional structures, has attracted increasingly attention in different fields such as capacitors, sensor, electronic devices and composite materials [27–30], which could be attributed to its all kinds of merits concluding large specific surface and carrier mobility [31, 32]. Moreover, Graphene oxide (GO), as a derivative of graphene, exhibits good conduction and light absorption for visible light [33]. Besides, the high single-layer charge mobility (2×105 $cm^2/(Vs)$) and good conductivity (1×10^2 S/m) were also important advantage of GO, owing to it features a conductive π–π conjugated structure [34]. GO can be usually prepared by thermal or chemical oxidation of graphene [35]. It goes without saying that GO could decrease efficiently the recombination rate of photoinduced charge carriers, and enhance the charge transfer rate of electrons, which could be ascribed to abundant oxygen-containing functional groups including hydroxyl, carboxyl and epoxy [36]. Therefore, in order to prepare high-active photocatalytic materials, GO will be the optimal choice in the near future.

Ultrasonic irradiation was a well-known technology which has been widely used in in various fields, and the effects of ultrasonic irradiation on the mechanical, physical, and chemical changes of materials have also received broad attention. Generally speaking, the effects induced by ultrasound in aqueous solution have been attributed to the collapse of cavitation bubbles, which generate extreme temperatures and pressures around the solid–liquid interfaces [37]. These local effects produce a variety of radicals and highly active intermediates, which may then initiate or induce material modifications [38]. More importantly, compared with the traditional homogeneous precipitation, the ultrasound-assisted precipitation could better control product particle size and the size distribution [39]. Studies on the synthesis of AgBr/GO composite by in situ growth method have been reported [40, 41], but as far as we know, there were relatively few reports on the use of ultrasonic during precipitation of AgBr/GO synthesis.

Based on the above discussion, AgBr/GO nanocomposite was successfully prepared through a single step ultrasonic chemical precipitation approach. As we expected, the modification with GO could significantly enhance the PC performance for PCBA degradation under simulated sunlight irradiation, which is ascribed to the improved charge separation as the transfer of photogenerated electron is adjusted effectively. Moreover, the physicochemical properties of as-prepared samples were by investigated kinds of technologies, and the main active species to degrade the PCBA were explored on AgBr/GO nanocomposite by fluorescent technique. Additionally, we further elucidate the possible degradation pathways of PCBA through identifying the corresponding degradation intermediates. Consequently, the enhanced PC mechanism of AgBr/GO nanocomposite is also discussed in detail. This work would provide a more viable approach to improve the PC performances of AgBr/GO photocatalysts in the environmental restoration and energy conversion.

2.1 Synthesis of AgBr/GO nanocatalyst

In the study, all chemicals were of analytical grade and without further purification before use. De-ionized water was employed throughout all experiments. According to modified Hummers' method, the graphene oxide (GO) was prepared from pristine graphite [42]. The AgBr/GO nanocatalyst was synthesized by one-step ultrasonic chemical precipitation method. Typically, 0.35 g GO was dispersed in 100 mL deionized water under ultrasonic treatment (300 W). Afterwards, 60 mL of silver nitrate ($AgNO_3$) with a concentration of 0.05 mol L^{-1} was added above solution and then continuously stirred for 40 min. Then, 20 mL of sodium bromide (0.05 mol L^{-1}) was dropwise instilled into the above mixture solution. Notably, the emulsion was ultrasonicated for 60 min. Subsequently, the as-formed yellowish precursor was centrifuged and rinsed repeatedly using ultrapure water and absolute ethanol. Eventually, as-prepared samples were dried at in the oven at 378 K for 2 h. The obtained sample was denoted as AgBr/GO nanocatalyst. For comparison, the AgBr nano-particles were also fabricated without the existence of GO under the same procedure.

2.2 Characterization

The crystal phases of the obtained products were collected on a Rigaku D/MAX III-3B diffractometer (Cu Kα radiation, $\lambda = 0.15418$ nm) with the accelerating potential of 40 kV and applied current of 30 mA in a 2θ range from 5° to 80° at room temperature. The morphologies of as-prepared samples were seen by a Quanta 200F field emission scanning electron microscope (FE-SEM) at 20 kV and transmission electron microscope (TEM, F-30ST, Tecnai) at an accelerating voltage of 300 kV. Raman spectrum was conducted by using a Jobin Yvon HR800 Raman spectrophotometer (equipped with Ar laser excitation wavelength of 457.9 nm). UV–Vis diffuse reflectance spectra (DRS) were carried out with a UV–Vis spectrophotometer (UV-2550) using $BaSO_4$ as reference. Time-resolved surface photovoltage (TRSPV) responses and surface photovoltage spectroscopy (SPS) of

the samples were carried out with a home-built apparatus. Hydroxyl (·OH) radicals at the photo-illuminated material/water interface was detected by the fluorescence characteristics using a FP-6500 fluorescence spectrometer.

2.3 Photoelectrochemical (PECH) measurements

The transient photocurrent density response and EIS curves of samples were measured on a PQSTA 128 N electrochemical workstation in a traditional three-electrode configuration with as-prepared AgBr/GO electrode, Pt plate and saturated calomel electrode (SCE) as the working electrode, counter electrode and reference electrode, respectively. Noted, 0.1 mol·L^{-1} of sodium sulfate was used as the supporting electrolyte.

2.4 Photocatalytic degradation experiments

The PC activities of the as-prepared samples were investigated through the photodegradation of refractory parachlorobenzoic-acid (PCBA) irradiated by a 35 W Xe lamp with illumination intensity of 67 mW cm^{-2} in a self-made cylindrical quartz reactor. In a typical experiment, 0.01 g photocatalyst was added into 50 mL of PCBA solution (5 mg L^{-1}). Before exposed to visible light, the suspension was magnetically stirred in dark for 30 min to ensure that the adsorption/desorption equilibrium of pollutions on the surface of the AgBr/GO nanocatalyst had been reached. After that, a 35 W Xenon lamp with similar sunlight emission spectra was turned on. At regular intervals, an aliquot (4 mL) was withdrawn with centrifugation to separate solids and measured the residual pollutant concentration by a Shimadzu LC 10 A high performance liquid chromatography (HPLC) equipped with a Kromasil KR100-5 C18 column (20 mm × 4.6 mm i.d.). Moreover, the degradation efficiency was calculated according to $\eta = (C_t - C_0)/C_0$, where η, C_t and C_0 is the degradation efficiency, the concentration of reactant at the time of t and 0, respectively.

The microcosmic surface morphologies of pristine AgBr and AgBr/GO nanocatalysts were studied by SEM and TEM. As shown in Fig. 1a, it can be observed that the pristine AgBr presented a great deal of spherical nanoparticles and aggregated irregularly. By measurement and evaluation, the diameter of nanoparticles was in the range of 200–400 nm. However, after the GO introduced into the reaction system, seen from Fig. 1b, the distribution of AgBr nanoparticles on the surface of GO was more uniform compared with that of pristine AgBr nanoparticles, which was mainly ascribed to the coaction of between oxygen-functional groups and OH groups from GO. Moreover, TEM images of AgBr/GO nanocatalyst were displayed in Fig. 1c. Clearly, AgBr nanoparticles were successfully decorated onto the surface of GO. The HR-TEM image in Fig. 1d taken at the interface of AgBr/GO nanocatalyst evidently exhibited series of typical fringes. The sample showed interplanar spacing of 0.288 nm, which were indexed to the (200) plane of AgBr [43], implying that AgBr nanoparticles were well-decorated on or combined with the GO sheets. Due to the interaction of between GO and AgBr in the nanocomposites, it is responsible for carrier transport at the interface offering sufficient contacting surface and also good potential.

The crystal phase structures of pristine AgBr, GO and AgBr/GO nanocatalyst were confirmed by XRD technique. As displayed in Fig. 2, noticeably, the pattern for GO have a major peak that can be well-indexed to (001) diffraction peak of interlayer spacing. The lattice distance calculated by Scherrer's equation is 0.886 nm. Some characteristic peaks of pristine AgBr can be seen at 26.7°, 30.97°, 44.32°, 52.57, 55.04°, 64.52° and 73.28° which can be well indexed to (111), (200), (220), (311), (222), (400) and (420) planes of the AgBr phase (JCPDS no. 79-0149) [44], respectively. More importantly, When AgBr was decorated on the surface of GO nanosheets, the crystal structures of AgBr/GO composite were almost changeless compared with that of the pristine AgBr nanoparticles, suggesting that the lattice of AgBr weren't incorporated by GO. In addition, no impurity peaks were observed, confirming the high purity of the products. Wondrously, the diffraction peaks of GO from AgBr/GO composites cannot be observed in the patters owning to a small quantity of decorated GO with a low atomic number cannot be detected by XRD. Thus, it can be reasonable deduction that AgBr/GO composites were successfully prepared by a single step ultrasonic chemical precipitation approach, which was consisting with the SEM and TEM results.

In order to obtain better confirmation on the presence of GO and AgBr, Raman spectroscopic investigation was also conducted. The Raman spectra of GO and AgBr/GO composites were displayed in Fig. 3. Obviously, In the Raman spectrum of GO, two typical bands of GO can be found at 1366 and 1590 cm^{-1}, corresponding to the well documented D and G bands [45], respectively. However, the D-bands underwent a significant shift toward higher frequencies from 1366 cm^{-1} to 1368 cm^{-1} accompanied by peak broadening for the AgBr/GO composites and became weaker than that of GO, indicating a portion of GO are changed due to the introduction of AgBr nanoparticles. Furthermore, the D/G integral intensity ratio (I_D/I_G) for GO in the AgBr/GO composites (0.86) is lower than that of GO (0.93), which is due to a certain amount of oxygen functional groups in the GO from AgBr/GO composites increase during the ultrasonic chemical precipitation process, and the conjugated GO

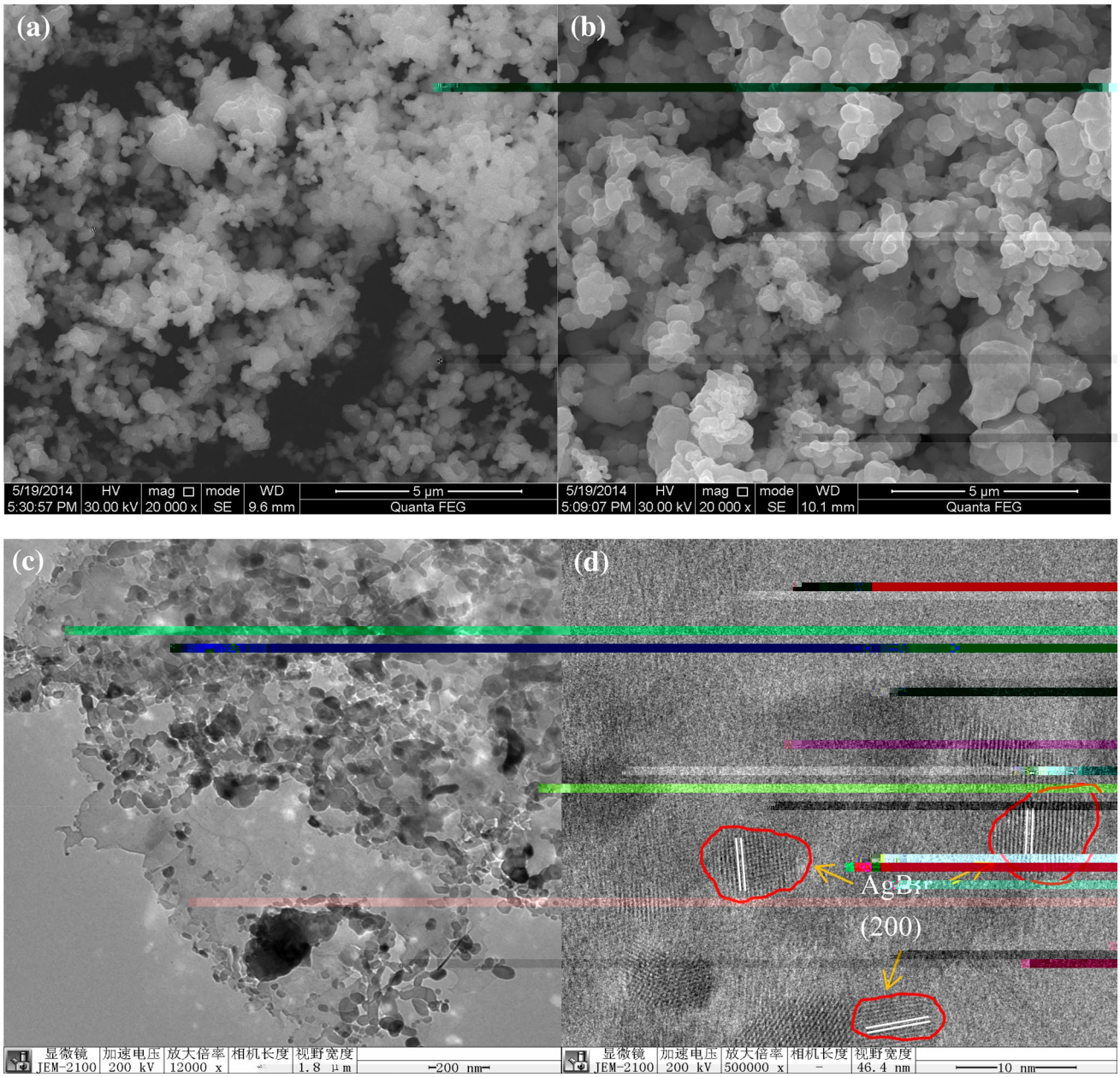

Fig. 1 SEM images of AgBr (**a**) and AgBr/GO (**b**); TEM image (**c**) and high-amplifying image (**d**) of AgBr/GO nano-catalysts

networks were reestablished [46, 47]. As a consequence, it can reasonably be concluded that AgBr nanoparticles are successfully loaded onto GO nanosheets, allowing it to become a possibility for improving charge transfer in the interface of between AgBr and GO in AgBr/GO composites.

In order to investigate the optical absorption property of as-prepared samples, the UV–Vis diffuse reflectance spectra of pristine AgBr and AgBr/GO nanocatalyst were measured and recorded in Fig. 4. As we all know, the absorption range of light plays an important role in the photocatalysis, especially for the visible-light photodegradation [48]. Seen from Fig. 4a, the primary absorption edge of pristine AgBr occurred at 470 nm. However, a significantly enhanced absorption between UV and visible light for AgBr/GO nanocatalyst was clearly seen. This is attributed to the strong absorption of GO in the visible-light region, which contributes to the great light harvesting efficiency of AgBr/GO nanocatalyst. Moreover, for AgBr/GO nanocatalyst, the absorption edge of presented at 520 nm and the light absorption was greatly improved through bathochromic shift for the band gap transition. Also, the band gap energy can be evaluated with the following equations: $ah\nu = A(\alpha h\nu - Eg)^{n/2}$.

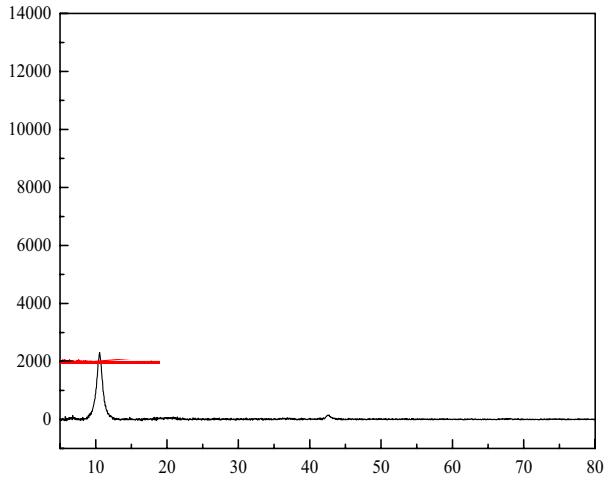

As displayed in Fig. 4b, AgBr and AgBr/GO nanocatalyst exhibit band gap energy of 2.36 eV and 1.95 eV, respectively. The band gap of AgBr/GO nanocatalyst narrowed by 0.41 eV compared with AgBr, clearly, the introduction of GO will exert significant impact on the optoelectronic behavior of as-prepared materials. That was to say, AgBr/GO nanocomposite could efficiently utilize visible light and produce more photo-induced electron–hole pairs under visible light illumination. Results also testified that a large amount of electrons and holes could be photogenerated for AgBr/GO nanocatalyst to take part in the desired PC reaction as more visible light absorption.

The surface photovoltage spectra (SPS) and time-resolved surface photovoltage (TR-SPV) responses are regarded as an effective approach to investigate the nature of photogenerated charges in solid-state semiconductors [19]. The separation ability of the photogenerated electron–hole pairs could be directly reflected by the intensity of the SPS signal, and the TR-SPV signal reflects the lifetime of the photogenerated carriers in the semiconductor material [49]. In general, the stronger SPS response meant the higher separation efficiency of photoproduced charge. As shown in Fig. 5a, clearly, it can be seen that the SPS intensity of AgBr/GO nanocomposite was apparently higher than that of pure AgBr, indicating the enhanced charge separation due to the introduction of GO that possessed various oxygen-containing functional groups. Moreover, the TR-SPV responses of AgBr and AgBr/GO nanocomposite were investigated and shown in Fig. 5b. One can notice that there were positive TR-SPV responses for AgBr and AgBr/GO nanocomposite, implying that positive holes were generated, separated and then collected on the

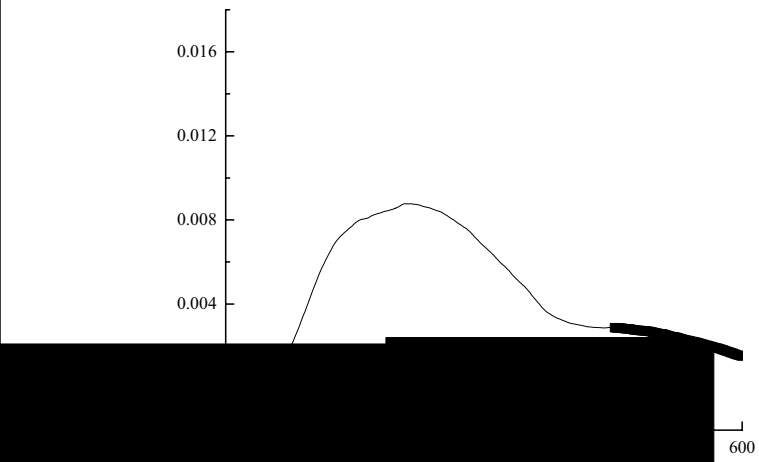

ed for
cates
usion
ction
/GO
AgBr,
hoto-
r/GO
arrier
Based
nano-
ement

o-cat-
AgBr.
pho-
urrent
vever,

when the light was switched on, the transient photocurrent instantly increase to the maximum value, and then it slightly declines (transient photocurrent decay) before reaching the equilibrium. Clearly, AgBr/GO nano-catalyst not only maintained the original value, but also exhibited relatively high stability after several times switch the light cycles of an interrupted 35 W Xenon lamp irradiation. In addition, the transient photocurrent intensity of AgBr/GO nano-catalyst was obviously higher than that of pristine AgBr, which exhibited greatly the improvement of separation efficiency of photoinduced charge carriers and higher PC activity, owning to the interaction of between AgBr and GO resulting in the higher response of visible light for AgBr/GO composites.

To better understand the separation efficiency of photogenerated charge carrier, electrochemical impedance spectra (EIS) was also be conducted by electrochemical workstation at the open circuit potential in dark and under irradiation, respectively. The Nyquist plots from the EIS

measurement of pristine AgBr and AgBr/GO nanocomposite were shown in Fig. 6b. As we all know, the charge transfer rate can be determined from the arc diameter of the Nyquist plot. That is to say, the smaller semicircle in the Nyquist plots indicated higher charge carrier transfer efficiency. The AgBr and AgBr/GO nanocomposite showed the smaller arc radius under the identical visible-light irradiation compared with that of in the dark, respectively, which revealed a greatly enhanced charge carrier separation and transfer under light irradiation. In addition, AgBr/GO nanocomposite possessed much smaller radius of the semicircle than that of pristine AgBr with or without a 35 W Xenon lamp irradiation, respectively. Therefore, the low interfacial charge transfer resistance achieving by the AgBr/GO nanocomposite suggested the separation and transfer of photo-generated carriers would be accelerated and the PC activities would be improved. The finding about EIS analysis was consistent well with results obtained by the PC activities evaluation.

It is proved that the generated hydroxyl (˙OH) radical takes the dominant position in the PC reaction [50]. Moreover, the recombination of photoinduced e/h^+ pair was inevitable at the surface or trapping centers with the release of photons and heat for most of semiconductor materials. Thus, to investigate separation efficiency of photoinduced e/h^+ pairs, FL technique, as a reliable technique, was used to study the production of hydroxide radical (˙OH). The fluorescence spectra related to the produced ˙OH amount are shown in Fig. 7. Clearly, it can be observed that the FL intensity of AgBr/GO nanocomposite was stronger than that of pristine AgBr under visible light irradiation. The higher comparative FL intensity meant more amount of ˙OH radicals produced by AgBr/GO nanocomposite. Thus, the introduction of GO would remarkably promote the absorption of visible light and enhance separation efficiency of photoexcited charge carriers resulting in the higher PC activity, which was consistent with the aforementioned results.

In the research, parachlorobenzoic-acid (PCBA) was used as target pollutant to evaluate the PC performances of AgBr/GO nanocomposite and the result was shown in Fig. 8a. The visible light source was provided by a 35 W Xenon lamp with illumination intensity of 67 mW cm^{-2}. Meanwhile, PC activities of pristine AgBr and TiO_2 were also measured for reference. Obviously, PCBA was hardly decomposed through direct photolysis without AgBr/GO nanocomposite and adsorption in dark with AgBr/GO nanocomposite. When the TiO_2 was used as catalyst, 10.3% of PCBA was decomposed within 50 min, while the AgBr can degrade 61.1% of PCBA under the same condition. Besides, the degradation rate of PCBA on AgBr/GO nanocomposite reached 99.9% within 40 min Xenon lamp illumination, which was 1.6 and 9.7 times as high as that of the pristine AgBr and TiO_2, respectively. Moreover, the degradation of PCBA can be modeled by a Langmuir–Hinshelwood (L–H) model with a pseudo-first-order kinetics. Apparently, seen from Fig. 8b, the kinetic constant of AgBr/GO nanocomposite was the

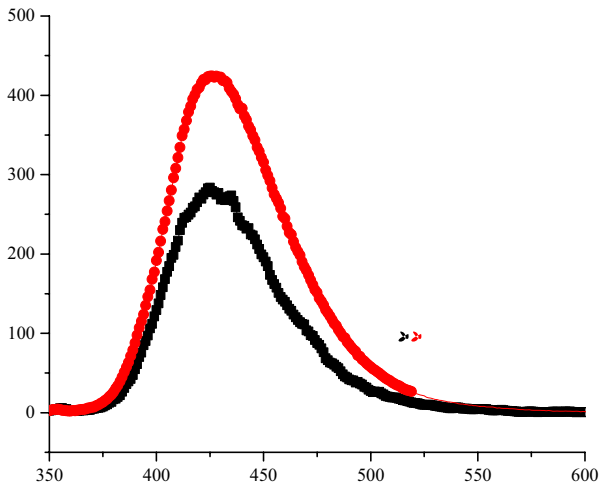

highest among all materials. Therefore, it played key roles for the visible-light-induced PC reaction because the introduction of GO greatly improved visible light absorbance, promoted the transfer of photo-produced electron.

On the basis of the above-mentioned analysis, the enhancement of the photocatalytic activity of the AgBr/GO nanocomposite can be well interpreted. The proposed mechanism for PCBA photocatalytic degradation was shown in Fig. 9. The GO can easily captured pollutant molecules in the solution owning to its various oxygen-function groups. Moreover, when AgBr/GO nanocomposite was illuminated by visible light, the electrons from VB of AgBr can be motivated rapidly to CB of AgBr in the photocatalytic reaction process. The photogenerated electrons can transfer to the GO surface due to the Schottky barriers, which facilitates the electron–hole pair separation. These electrons on the surface of GO reduce the dissolved oxygen, leading to the formation of O^{2-}. Thus, the introduction of GO can increase the rate of formation of O^{2-}, while simultaneously decreasing the rate of recombination. In the final state, the

In summary, the preparation of AgBr/GO nanocomposite was successfully achieved through a single step ultrasonic chemical precipitation approach. Subsequently, the physicochemical properties of as-prepared samples were systematically studied through SEM, TEM, XRD, Raman, UV–Vis DRS, TRSPV, SPS and PECH measurements. In comparison of single-phase, the as-obtained AgBr/GO composite photocatalyst exhibited extend light absorbance performance and higher transient photocurrent density, which could be explained as that the modification with graphene oxide could greatly enhance the photogenerated charge separation of AgBr nano-catalysts by effectively capturing photoproduced charge. It is well responsible for the obviously-improved photocatalytic activities for degrading organic pollutants. Results about the degradation of PCBA indicated that AgBr/GO nanocomposite showed much greater photocatalytic activity (99.9%) compared with that of TiO_2 (10.3%) and pristine AgBr (61.1%). The origin of this effectiveness was shown to emerge from improved absorption in the visible light range possibly due to the interaction of between AgBr and GO. Moreover, the formed $^{\cdot}OH$ could dominate mainly the photocatalytic degradation of PCBA for AgBr/GO nanocomposite. In addition, the main possible pathways for decomposition of PCBA under Xenon lamp illumination were proposed. Thus, this research would provide a feasible strategy to improve the photocatalytic activities of AgBr/GO nanocomposite for environmental remediation. More importantly, it can help us to well understand the significance to increase the conductivity of photogenerated electrons for efficient photocatalysis on AgBr/GO nanocomposite.

Acknowledgements This work was kindly supported by National Natural Science Foundation of China (51808062, 51608061).

1. S.S. Xue, H.B. He, Z. Wu, C.L. Yu, Q.Z. Fan, G.M. Peng, K. Yang, An interesting Eu, F-codoped $BiVO_4$ microsphere with enhanced photocatalytic performance. J. Alloys Compd. **694**, 989–997 (2017)
2. G. Zerjav, M.S. Arshad, P. Djinovic, J. Zavasnik, A. Pintar, Electron trapping energy states of TiO_2-WO_3 composites and their influence on photocatalytic degradation of bisphenol A. Appl. Catal. B **209**, 273–284 (2017)
3. R. Zouzelka, J. Rathousky, Photocatalytic abatement of NOx pollutants in the air using commercial functional coating with porous morphology. Appl. Catal. B **217**, 466–476 (2017)
4. Y.J. Zou, J.W. Shi, D.D. Ma, Z.Y. Fan, L. Lu, C.M. Niu, In situ synthesis of C-doped TiO_2@g-C_3N_4 core-shell hollow nanospheres with enhanced visible-light photocatalytic activity for H_2 evolution. Chem. Eng. J. **322**, 435–444 (2017)
5. S.C. Wu, C.S. Tan, M.H. Huang, Strong facet effects on interfacial charge transfer revealed through the examination of photocatalytic activities of various Cu_2O-ZnO heterostructures. Adv. Funct. Mater. **27**, 1604635 (2017)
6. D.W. Park, K. Lee, J.C. Chae, T. Kudo, C.K. Kim, Genetic structure of xyl gene cluster responsible for complete degradation of (4-chloro)benzoate from *Pseudomonas* sp. S-47. J. Microbiol. Biotechnol. **14**, 483–489 (2004)
7. C. Creaser, L.F. dos Santos, D.G. Lamarca, A. New, J.C. Wolff, Biodegradation studies of 4-fluorobenzoic acid and 4-fluorocinnamic acid: an evaluation of membrane inlet mass spectrometry as an alternative to high performance liquid chromatography and ion chromatography. Anal. Chim. Acta **454**, 137–145 (2002)
8. H.R. Yi, K.H. Min, C.K. Kim, J.O. Ka, Phylogenetic and phenotypic diversity of 4-chlorobenzoate-degrading bacteria isolated from soils. FEMS Microbiol. Ecol. **31**, 53–60 (2000)
9. E.C. Wert, S. Gonzales, M.M. Dong, F.L. Rosario-Ortiz, Evaluation of enhanced coagulation pretreatment to improve ozone oxidation efficiency in wastewater. Water Res. **45**, 5191–5199 (2011)
10. Y.H. Dao, J. De Laat, Hydroxyl radical involvement in the decomposition of hydrogen peroxide by ferrous and ferric-nitrilotriacetate complexes at neutral pH. Water Res. **45**, 3309–3317 (2011)
11. R.M. El-Sherif, T.A. Lasheen, E.A. Jebril, Fabrication and characterization of CeO_2-TiO_2-Fe_2O_3 magnetic nanoparticles for rapid removal of uranium ions from industrial waste solutions. J. Mol. Liq. **241**, 260–269 (2017)
12. F.J. Chen, P.L. Ho, R. Ran, W.M. Chen, Z.C. Si, X.D. Wu, D. Weng, Z.H. Huang, C. Lee, Synergistic effect of CeO_2 modified TiO_2 photocatalyst on the enhancement of visible light photocatalytic performance. J. Alloys Compd. **714**, 560–566 (2017)
13. S. Riyas, P.N.M. Das, Effect of Fe_2O_3 and Cr_2O_3 on anatase-rutile transformation in TiO_2. Br. Ceram. Trans. **103**, 23–28 (2004)
14. S. Byun, B. Kim, S. Jeon, B. Shin, Effects of a SnO_2 hole blocking layer in a $BiVO_4$-based photoanode on photoelectrocatalytic water oxidation. J. Mater. Chem. A **5**, 6905–6913 (2017)
15. W. Ahmad, T. Noor, M. Zeeshan, Effect of synthesis route on catalytic properties and performance of Co_3O_4/TiO_2 for carbon monoxide and hydrocarbon oxidation under real engine operating conditions. Catal. Commun. **89**, 19–24 (2017)
16. S. Zou, S. Zhong, C. Lv, C. Wang, T. Chen, Z.J. Liu, S.Y. Zhang, Effect of synthesis highly ordered TiO_2 nanotube arrays with enhanced photocatalytic properties by time, electrolytic voltage, heating temperature and Polyvinyl pyrrolidone. J. Porous Mater. **23**, 1239–1247 (2016)
17. Y. Zhou, C.H. Chen, N.N. Wang, Y.Y. Li, H.M. Ding, Stable Ti^{3+} self-doped anatase-rutile mixed TiO_2 with enhanced visible light utilization and durability. J. Phys. Chem. C **120**, 6116–6124 (2016)
18. P. Zhang, Y. Liu, B.Z. Tian, Y.S. Luo, J.L. Zhang, Synthesis of core-shell structured CdS@CeO_2 and CdS@TiO_2 composites and comparison of their photocatalytic activities for the selective oxidation of benzyl alcohol to benzaldehyde. Catal. Today **281**, 181–188 (2017)
19. X.Z. Yue, S.S. Yi, R.W. Wang, Z.T. Zhang, S.L. Qiu, A novel architecture of dandelion-like Mo_2C/TiO_2 heterojunction photocatalysts towards high-performance photocatalytic hydrogen production from water splitting. J. Mater. Chem. A **5**, 10591–10598 (2017)
20. H.Z. Yao, W.Y. Fu, L. Liu, X. Li, D. Ding, P.Y. Su, S. Feng, H.B. Yang, Hierarchical photoanode of rutile TiO_2 nanorods coupled with anatase TiO_2 nanosheets array for photoelectrochemical application. J. Alloys Compd. **680**, 206–211 (2016)

21. P.H. Wang, Ag-AgBr/TiO_2/RGO nanocomposite: Synthesis, characterization, photocatalytic activity and aggregation evaluation. J. Environ. Sci. **56**, 202–213 (2017)
22. X.L. Miao, X.P. Shen, J.J. Wu, Z.Y. Ji, J.H. Wang, L.R. Kong, M.M. Liu, C.S. Song, Fabrication of an all solid Z-scheme photocatalyst g-C_3N_4/GO/AgBr with enhanced visible light photocatalytic activity. Appl. Catal. A **539**, 104–113 (2017)
23. W.Y. Gao, C.X. Ran, M.Q. Wang, L. Li, Z.W. Sun, X. Yao, The role of reduction extent of graphene oxide in the photocatalytic performance of Ag/AgX (X = Cl, Br)/rGO composites and the pseudo-second-order kinetics reaction nature of the Ag/AgBr system. Phys. Chem. Chem. Phys. **18**, 18219–18226 (2016)
24. P.H. Wang, Y.X. Tang, Z.L. Dong, Z. Chen, T.T. Lim, Ag-AgBr/TiO_2/RGO nanocomposite for visible-light photocatalytic degradation of penicillin G. J. Mater. Chem. A **1**, 4718–4727 (2013)
25. Y.Y. Bai, F.R. Wang, J.K. Liu, A new complementary catalyst and catalytic mechanism: Ag_2MoO_4/Ag/AgBr/GO heterostructure. Ind. Eng. Chem. Res. **55**, 9873–9879 (2016)
26. A. Esmaeili, M.H. Entezari, Sonosynthesis of an Ag/AgBr/Graphene-oxide nanocomposite as a solar photocatalyst for efficient degradation of methyl orange. J. Colloid Interface Sci. **466**, 227–237 (2016)
27. H. Naderi, A. Sobhani-Nasab, M. Rahimi-Nasrabadi, M. Ganjali, Decoration of nitrogen-doped reduced graphene oxide with cobalt tungstate nanoparticles for use in high-performance supercapacitors. Appl. Surf. Sci. **423**, 1025–1034 (2017)
28. A. Khoshroo, L. Hosseinzadeh, A. Sobhani-Nasab, M. Rahimi-Nasrabadi, H. Ehrlich, Development of electrochemical sensor for sensitive determination of oxazepam based on silver-platinum core–shell nanoparticles supported on graphene. J. Electroanal. Chem. **823**, 61–66 (2018)
29. J. Amani, M. Maleki, A. Khoshroo, A. Sobhani-Nasab, M. Rahimi-Nasrabadi, An electrochemical immunosensor based on poly p-phenylenediamine and graphene nanocomposite for detection of neuron-specific enolase via electrochemically amplified detection. Anal. Biochem. **548**, 53–59 (2018)
30. M. Rostami, M. Rahimi-Nasrabadi, M.R. Ganjali, F. Ahmadi, A.F. Shojaei, M.D. Rafiee, Facile synthesis and characterization of TiO_2-graphene-$ZnFe_2$-xTb_x O_4 ternary nano-hybrids. J. Mater. Sci. **52**, 7008–7016 (2017)
31. P.Q. Wang, T. Chen, B.Y. Yu, P. Tao, Y. Bai, Tollen's-assisted preparation of Ag_3PO_4/GO photocatalyst with enhanced photocatalytic activity and stability. J. Taiwan Inst. Chem. Eng. **62**, 267–274 (2016)
32. Z.Y. Ji, J.L. Zhao, X.P. Shen, X.Y. Yue, A.H. Yuan, H. Zhou, J. Yang, Construction of magnetically separable Ag_3PO_4/Fe_3O_4/GO composites as recyclable photocatalysts. Ceram. Int. **41**, 13509–13515 (2015)
33. W.Y. Zhu, F.Q. Sun, R. Goei, Y. Zhou, Facile fabrication of RGO-WO_3 composites for effective visible light photocatalytic degradation of sulfamethoxazole. Appl. Catal. B **207**, 93–102 (2017)
34. F.Y. Chen, W.,J. An, L. Liu, Y.H. Liang, W.Q. Cui, Highly efficient removal of bisphenol A by a three-dimensional graphene hydrogel-AgBr@rGO exhibiting adsorption/photocatalysis synergy. Appl. Catal. B **217**, 65–80 (2017)
35. X.L. Yang, F.F. Qian, Y. Wang, M.L. Li, J.R. Lu, Y.M. Li, M.T. Bao, Constructing a novel ternary composite $(C_{16}H_{33}(CH_3)_{(3)}N_{(4)}W_{10}O_{32}$/g-$C_3N_4$/rGO with enhanced visible-light-driven photocatalytic activity for degradation of dyes and phenol. Appl. Catal. B **200**, 283–296 (2017)
36. A. Omidvar, B. Jaleh, M. Nasrollahzadeh, Preparation of the GO/Pd nanocomposite and its application for the degradation of organic dyes in water. J. Colloid Interface Sci. **496**, 44–50 (2017)
37. S. Tangestaninejad, V. Mirkhani, M. Moghadam, I. Mohammadpoor-Baltork, E. Shams, H. Salavati, Hydrocarbon oxidation catalyzed by vanadium polyoxometalate supported on mesoporous MCM-41 under ultrasonic irradiation. Ultrason. Sonochem. **15**, 438–447 (2008)
38. W.F. Liu, J. Zhang, C. Cheng, G.P. Tian, C.L. Zhang, Ultrasonic-assisted sodium hypochlorite oxidation of activated carbons for enhanced removal of Co(II) from aqueous solutions. Chem. Eng. J. **175**, 24–32 (2011)
39. P. Kim-Lohsoontorn, C. Paichitra, S. Vorathamthongdee, P. Seeharaj, Low-temperature preparation of $BaCeO_3$ through ultrasonic-assisted precipitation for application in solid oxide electrolysis cell. Chem. Eng. J. **278**, 13–18 (2015)
40. H.R. Wang, L. Zou, Y.C. Shan, X. Wang, G.O. Ternary, Ag_3PO_4/AgBr composite as an efficient visible-light-driven photocatalyst. Mater. Res. Bull. **97**, 189–194 (2018)
41. X.L. Miao, X.P. Shen, J.J. Wu, Z.Y. Jia, J.H. Wang, L.R. Kong, M.M. Liu, C.S. Song, Fabrication of an all solid Z-scheme photocatalyst g-C_3N_4/GO/AgBr with enhanced visible light photocatalytic activity. Appl. Catal. A **539**, 104–113 (2017)
42. X. Zhang, P.S. Kumar, V. Aravindan, H.H. Liu, J. Sundaramurthy, S.G. Mhaisalkar, H.M. Duong, S. Ramakrishna, S. Madhavi, Electrospun TiO_2-graphene composite nanofibers as a highly durable insertion anode for lithium ion batteries. J. Phys. Chem. C **116**, 14780–14788 (2012)
43. B. Feng, Z.Y. Wu, J.S. Liu, K.J. Zhu, Z.Q. Li, X. Jin, Y.D. Hou, Q.Y. Xi, M.Q. Cong, P.C. Liu, Q.L. Gu, Combination of ultrafast dye-sensitized-assisted electron transfer process and novel Z-scheme system: AgBr nanoparticles interspersed MoO_3 nanobelts for enhancing photocatalytic performance of RhB. Appl. Catal. B **206**, 242–251 (2017)
44. D.D. Yu, J. Bai, H. Liang, C.P. Li, Electrospinning, solvothermal, and self-assembly synthesis of recyclable and renewable AgBr-TiO_2/CNFs with excellent visible-light responsive photocatalysis. J. Alloys Compd. **683**, 329–338 (2016)
45. J.Y. Si, Y. Liu, S.Z. Chang, D. Wu, B.Z. Tian, J.L. Zhang, AgBr@TiO_2/GO ternary composites with enhanced photocatalytic activity for oxidation of benzyl alcohol to benzaldehyde. Res. Chem. Intermed. **43**, 2067–2080 (2017)
46. B.Q. Lu, N. Ma, Y.P. Wang, W.Q. Yi, H.H. Hu, J.H. Zhao, D.Y. Liang, S. Xu, X.Y. Li, Z.Y. Zhu, C. Cui, Visiblelightdriven TiO_2/Ag_3PO_4/GO heterostructure photocatalyst with dual-channel for photo-generated charges separation. J. Alloys Compd. **630**, 163–171 (2015)
47. X.Y. Zhang, H.P. Li, X.L. Cui, Y.H. Lin, Graphene/TiO_2 nanocomposites: synthesis, characterization and application in hydrogen evolution from water photocatalytic splitting. J. Mater. Chem. **20**, 2801–2806 (2010)
48. C.F. Liu, C.P. Huang, C.C. Hu, Y.J. Juang, C.P. Huang, Photoelectrochemical degradation of dye wastewater on TiO_2-coated titanium electrode prepared by electrophoretic deposition. Sep. Purif. Technol.

0002 2 4000001 ca b s 02 a 20 70 a a 683 104 113 2017 42